

# Visualizing Galectin-3 Binding Protein Expression with ImmunoPET

Outi Keinänen, Samantha M. Sarrett, Samantha Delaney, Cindy Rodriguez, Eric J. Dayts, Emily Capone, Frederic Saunier, Rodolfo Ippoliti, Gianluca Sala, Stefano Iacobelli, and Brian M. Zeglis\*



Cite This: *Mol. Pharmaceutics* 2023, 20, 3241–3248



Read Online

ACCESS |



Metrics & More



Article Recommendations



Supporting Information

**ABSTRACT:** Galectin-3 binding protein (Gal-3BP) is a glycoprotein that is overexpressed and secreted by several cancers and has been implicated as a marker of both tumor progression and poor prognosis in melanoma, non-small cell lung cancer, head and neck squamous cell carcinoma, and breast cancer. The expression of Gal-3BP by a variety of neoplasms makes it an enticing target for both diagnostics and therapeutics, including immuno-positron emission tomography (immunoPET) probes and antibody-drug conjugates (ADCs). Herein, we report the development, *in vitro* characterization, and *in vivo* evaluation of a pair of Gal-3BP-targeting radioimmunoconjugates for  $^{89}\text{Zr}$ -immunoPET. A humanized anti-Gal-3BP antibody, 1959, and its corresponding ADC, 1959-sss/DM4 (DM4 = raptansine), were modified with desferrioxamine (DFO) to yield DFO-1959 and DFO-1959-sss/DM4 immunoconjugates bearing 1–2 DFO/monoclonal antibody. Both DFO-modified immunoconjugates retained their affinity for Gal-3BP in enzyme-linked immunosorbent assay experiments. The chelator-bearing antibodies were radiolabeled with zirconium-89 ( $t_{1/2} \approx 3.3$  d) to produce radioimmunoconjugates —  $^{89}\text{Zr}$ -DFO-1959 and  $^{89}\text{Zr}$ -DFO-1959-sss/DM4 — with high specific activity ( $>444$  MBq/mg,  $>12$  mCi/mg) and stability ( $>80\%$  intact after 168 h in human serum at  $37^\circ\text{C}$ ). In mice bearing subcutaneous Gal-3BP-secreting A375-MA1 xenografts,  $^{89}\text{Zr}$ -DFO-1959 clearly delineated tumor tissue, reaching a maximum tumoral activity concentration ( $54.8 \pm 15.8\%$  ID/g) and tumor-to-background contrast (tumor-to-blood =  $8.0 \pm 4.6$ ) at 120 h post-injection. The administration of  $^{89}\text{Zr}$ -DFO-1959 to mice bearing subcutaneous Gal-3BP-expressing melanoma patient-derived xenografts produced similarly promising results.  $^{89}\text{Zr}$ -DFO-1959 and  $^{89}\text{Zr}$ -DFO-1959-sss/DM4 exhibited nearly identical pharmacokinetic profiles in the mice bearing A375-MA1 tumors, though the latter produced higher uptake in the spleen and kidneys. Both  $^{89}\text{Zr}$ -DFO-1959 and  $^{89}\text{Zr}$ -DFO-1959-sss/DM4 effectively visualized Gal-3BP-secreting tumors in murine models of melanoma. These results suggest that both probes could play a role in the clinical imaging of Gal-3BP-expressing malignancies, particularly as companion theranostics for the identification of patients likely to respond to Gal-3BP-targeted therapeutics such as 1959-sss/DM4.

**KEYWORDS:** galectin-3 binding protein, positron emission tomography, immunoPET, theranostic imaging, Zr-89, antibody-drug conjugate

## INTRODUCTION

Galectin-3 binding protein — Gal-3BP; also known as LGALS3BP, 90K, or Mac-2-Binding Protein (Uniprot ID: Q08380) — is a highly glycosylated oligomeric protein that was originally identified in the conditioned medium of human breast cancer cells.<sup>1</sup> Gal-3BP is produced at low levels by healthy cells and tissues, but dramatically increased expression levels have been found in the tumors of patients with a variety of malignancies.<sup>2–6</sup> Gal-3BP expression and secretion have been shown to be markers of poor prognosis in breast cancer, non-small cell lung cancer, head and neck squamous cell carcinoma, and melanoma.<sup>3,4,7–10</sup> Along these lines, Gal-3BP is believed to be a driving force in several processes leading to cell transformation and tumor progression, including the regulation of adhesion processes, the stimulation of tumor angiogenesis, and the induction of immune escape.<sup>5,8,11,12</sup> Several groups have also identified Gal-3BP as a major component of cancer-derived extracellular vesicles (EVs).<sup>13–16</sup>

The expression of Gal-3BP by a variety of cancers has made it a particularly enticing target for the development of therapeutics. Indeed, an antibody-drug conjugate (ADC) based on the Gal-3BP-targeting monoclonal antibody (mAb)

1959 (i.e., 1959-sss/DM3 (DM3 = maytansinoid DM3)) has recently been shown to suppress tumor growth and prolong survival in murine models of melanoma and neuroblastoma.<sup>17,18</sup> In mice bearing melanoma xenografts, for example, a dose of 10 mg/kg 1959-sss/DM3 completely halted tumor growth and resulted in the survival of 100% of mice after 150 days, all with no observed mortality or treatment-related toxicity. The efficacy of 1959-sss/DM3 is especially remarkable given that Gal-3BP is secreted and that the ADC itself is non-internalizing. While conventional wisdom has held that ADCs must be internalized to efficiently deliver their toxic cargo, several recent studies have underscored the potential of non-internalizing ADCs — including the family based on 1959 — that target tumor- or stroma-associated antigens and exploit

**Received:** March 20, 2023

**Revised:** April 25, 2023

**Accepted:** April 26, 2023

**Published:** May 16, 2023



the reducing nature of the tumor microenvironment to release disulfide-linked toxins that can then diffuse into nearby tumor cells.<sup>19–21</sup>

Over the last two decades, ADCs have emerged as a highly promising class of therapeutics, with several gaining Food and Drug Administration (FDA) approval and many more in the clinical pipeline.<sup>22,23</sup> Yet the biochemical complexity of human tumors means that the accurate selection of patients likely to respond to ADC therapy is critical. PET imaging — and particularly immunoPET using mAbs labeled with zirconium-89 (<sup>89</sup>Zr;  $t_{1/2} \approx 3.3$  d) — has shown great promise in the preclinical development and clinical deployment of ADCs.<sup>24,25</sup> The ZEPHIR trial, for example, clearly demonstrated that theranostic immunoPET with <sup>89</sup>Zr-trastuzumab can help delineate patients likely to respond to therapy with trastuzumab emtansine: investigators found that patients in the “positive” immunoPET group exhibited a median time-to-treatment failure (TTF) of 11.2 months compared to 3.5 months for those in the “negative” immunoPET group.<sup>26</sup>

Herein, we report the synthesis, characterization, and *in vivo* evaluation of two Gal-3BP-targeting radioimmunoconjugates: [<sup>89</sup>Zr]Zr-DFO-1959 and [<sup>89</sup>Zr]Zr-DFO-1959-sss/DM4 (DFO = desferrioxamine). While Gal-3BP is a secreted antigen, high concentrations of the protein remain in close proximity to tumor cells.<sup>17,18</sup> Indeed, the feasibility of targeting shed antigens for immunoPET has already been demonstrated with several biomarkers, most notably CA19-9, CA-125, and VEGF-A.<sup>27–29</sup> In the end, our probes demonstrated highly promising *in vivo* behavior in two murine models of melanoma, suggesting that they could ultimately play an important role in the clinic as companion theranostic imaging agents.

## METHODS AND MATERIALS

**Materials.** Unless otherwise noted, all chemicals were purchased from commercial vendors and used without further purification. All water used was ultrapure (>18.2 MΩ cm at 25 °C), and dimethyl sulfoxide was of molecular biology grade (>99.9%). *p*-SCN-Bn-DFO was purchased from Macrocyclics, Inc. (Plano, TX). <sup>89</sup>Zr was produced via the <sup>89</sup>Y(*p,n*)<sup>89</sup>Zr reaction and purified at Memorial Sloan Kettering Cancer Center as [<sup>89</sup>Zr]Zr-oxalate in 1.0 M oxalic acid or bought from 3D Imaging (Little Rock, AR) as [<sup>89</sup>Zr]Zr-oxalate in 1.0 M oxalic acid. Human IgG (#I4506) was purchased from Sigma-Aldrich (St. Louis, MO). All *in vivo* experiments were performed in accordance with published protocols approved by the Institutional Animal Care and Use Committees of Hunter College, Weill Cornell Medical College, and Memorial Sloan Kettering Cancer Center. All instruments were calibrated and maintained according to standard quality control practices and procedures. UV–vis measurements were taken on a Shimadzu BioSpecNano Microvolume UV–vis Spectrophotometer (Shimadzu Scientific Instruments, Kyoto, Japan). Radioactivity was measured using a CRC-15R Dose Calibrator (Capintec, Inc., Ramsey, NJ), and biodistribution samples were counted on a calibrated Automatic Wizard<sup>2</sup>  $\gamma$ -counter (PerkinElmer, Inc., Waltham, MA). The radiolabeling of the immunoconjugate was monitored using glass-fiber, silica-impregnated instant thin-layer chromatography (iTLC) paper (Pall Corp., East Hills, NY) and analyzed on an AR-2000 radio-TLC plate reader using Winscan Radio-TLC software (Bioscan, Inc., Washington, DC). Matrix-assisted laser desorption/ionization time-of-flight (MALDI-ToF) mass spectrometry service was provided by the Alberta Proteomics

and Mass Spectrometry Facility (University of Alberta, Alberta, Canada).

**1959 and 1959-sss/DM4.** 1959 and 1959-sss/DM4 were produced as previously described.<sup>1,18</sup> Briefly, 1959 is a humanized variant of the murine Gal-3BP-binding antibody SP2, which itself was generated by immunizing mice with proteins secreted by CG-5 human breast cancer cells.<sup>1</sup> The production of 1959 was achieved by grafting the complementarity determining regions (CDRs) of SP2 onto a human IgG<sub>1</sub> scaffold, placing the recombinant genes into the pCDNA3.1 expression vector, transfecting Chinese Hamster Ovary-S cells, and purifying the antibody product using a Protein-A column.<sup>18</sup> 1959-sss/DM4 is a linker-less ADC wherein a pair of toxins (DM4, a derivative of maytansine) is site-specifically appended to free cysteine residues within a genetically engineered variant of 1959 (i.e., 1959-sss) in which the serine residues at positions 220, 226, and 229 of the heavy chain have been replaced with cysteines (US 2008/0305044 A1).<sup>18,30</sup>

**Bioconjugation.** 1959 (4.97 mg, 33 nmol) was dissolved in 128  $\mu$ L of Chelex-treated (Chelex 100 Resin, Bio-Rad Laboratories, Inc.) phosphate-buffered saline (Chelex PBS, pH 7.4), and the pH of the solution was adjusted to 8.8–9.0 with 0.1 M Na<sub>2</sub>CO<sub>3</sub>. Five equivalents of *p*-SCN-Bn-DFO (12.5  $\mu$ L, 10 mg/mL in DMSO) were added to the solution in small aliquots. The resulting solution was incubated at 37 °C for 1 h with shaking at 500 rpm. The DFO-modified antibody was then purified using size exclusion chromatography (Sephadex G-25 M, PD-10 column, GE Healthcare; dead volume: 2.5 mL, eluted with 2 mL of Chelex PBS, pH 7.4) and concentrated using centrifugal filtration units with a 50,000 Da molecular weight cutoff (Amicon Ultra 2 mL Centrifugal Filtration Units, MilliporeSigma Corp., Burlington, MA). DFO-1959 was obtained in an overall yield of 93% relative to the 1959 starting material. DFO-1959-sss/DM4 was prepared as described above with the following modifications: 1.1 mg (7.3 nmol) of 1959-sss/DM4 and 2.8  $\mu$ L of *p*-SCN-Bn-DFO (10 mg/mL in DMSO) were used (yield: 89%). DFO-huIgG was prepared as described above with the following modifications: 3.2 mg (21.3 nmol) of huIgG and 8.1  $\mu$ L of *p*-SCN-Bn-DFO (10 mg/mL in DMSO) were used (yield: 93%). Size exclusion high-performance liquid chromatography (SE-HPLC) was used to assess whether aggregates formed after modification. To this end, PBS pH 7.4 was used as a mobile phase with a flow rate of 0.75 mL/min on a Superdex 200 Increase 10/300 GL column (Cytiva, Global Life Sciences Solutions USA LLC, Marlborough, MA).

**Mass Spectrometry.** Matrix-assisted laser desorption/ionization (MALDI) mass spectrometry was used to determine the number of DFO moieties per antibody (Alberta Proteomics and Mass Spectrometry Facility, University of Alberta, Canada). The immunoconjugates were analyzed in triplicate using a Bruker Ultraflex MALDI-ToF/ToF (Bruker Daltonics GmbH). To this end, 1  $\mu$ L of each sample (1 mg/mL) was mixed with 1  $\mu$ L of sinapic acid (10 mg/mL in 50% acetonitrile/water and 0.1% trifluoroacetic acid). One  $\mu$ L of the sample/matrix solution was then spotted onto a stainless-steel target plate and allowed to air-dry. Ions were analyzed in positive mode, and external calibration was performed using a standard protein mixture (bovine serum albumin). The difference between the mass of each DFO-bearing immunoconjugate and its unmodified parent antibody was calculated, and the degree of labeling was determined via division by the mass of *p*-SCN-Bn-DFO.

**ELISA.** The binding of 1959, DFO-1959, 1959-sss/DM4, and DFO-1959-sss/DM4 to Gal-3BP was investigated via enzyme-linked immunosorbent assay (ELISA) with the D2 protein, a recombinant fragment of the lectin-binding region of Gal-3BP. D2 protein was diluted to 5  $\mu\text{g}/\text{mL}$  in PBS, and the wells of an ELISA plate (Nunc MaxiSorp flat-bottom 96 well plate, Fisher Scientific) were coated with 100  $\mu\text{L}/\text{well}$  for 2 h at room temperature. After a brief blocking period (40 min with PBS containing 10% fetal calf serum (FCS)), the immunoconjugates were diluted in blocking buffer (5  $\mu\text{g}/\text{mL}$ ), and 100  $\mu\text{L}/\text{well}$  were applied for 2 h at room temperature. The bound immunoconjugates were detected using 1:5000 horseradish peroxidase (HRP)-labeled anti-human IgG (JacksonImmunoResearch Laboratories, West Grove, PA). 3,3',5,5'-Tetramethylbenzidine (TMB) substrate was used to develop the bound horseradish peroxidase (HRP) secondary antibody, and the color reaction was stopped with 2 N  $\text{H}_2\text{SO}_4$  after 10 min. Optical densities at 450 nm were determined using a SpectraMax i3 plate reader (Molecular Devices). Binding data was collected in triplicate, averaged, and plotted.

**Radiolabeling.** A solution of [ $^{89}\text{Zr}$ ]Zr-oxalate (150.6 MBq, 4.07 mCi) in 1.0 M oxalic acid was adjusted to pH 7.0–7.5 with 1.0 M  $\text{Na}_2\text{CO}_3$ , resulting in a total volume of 110  $\mu\text{L}$ . After the bubbling of  $\text{CO}_2(\text{g})$  ceased, the  $^{89}\text{Zr}$  solution was added to the DFO-1959 solution (266  $\mu\text{g}$  in 29.2  $\mu\text{L}$  of Chelex PBS, pH 7.4). The resulting mixture was placed on an agitating thermomixer at 350 rpm for 20 min at 37  $^\circ\text{C}$ . The progress of the reaction was then assayed using radio-iTLC with an eluent of 50 mM ethylenediaminetetraacetic acid (EDTA) pH 5.0. The immunoconjugate was purified using size exclusion chromatography (Sephadex G-25 M, PD-10 column, GE Healthcare; dead volume: 2.5 mL, eluted with 500  $\mu\text{L}$  fractions of Chelex PBS, pH 7.4). The radiochemical purity of the final radiolabeled construct was assayed via radio-iTLC using 50 mM EDTA pH 5.0 as an eluent. In the radio-iTLC experiments, the radioimmunoconjugate remains at the baseline, while free  $^{89}\text{Zr}^{4+}$  cations and [ $^{89}\text{Zr}$ ]Zr-EDTA travel with the solvent front. For the radiolabeling of DFO-1959-sss/DM4, 100  $\mu\text{g}$  of the construct and 62.9 MBq (1.7 mCi) of [ $^{89}\text{Zr}$ ]Zr-oxalate (total volume of 59  $\mu\text{L}$ ) were used. For the radiolabeling of DFO-huIgG, 100  $\mu\text{g}$  of the construct and 33.3 MBq (0.9 mCi) of [ $^{89}\text{Zr}$ ]Zr-oxalate (total volume of 340  $\mu\text{L}$ ) were used.

**In Vitro Stability.** The stabilities of the radioimmunoconjugates with respect to loss of radioactivity and aggregation were investigated via incubation in human serum for 7 days at 37  $^\circ\text{C}$  ( $n = 3$ ) with shaking at 350 rpm. At 24, 72, 120, and 168 h, the radiochemical purity of the radiolabeled antibodies were determined in triplicate via radio-iTLC with an eluent of 50 mM EDTA pH 5.0. At 24 and 120 h, the stabilities of the constructs were monitored via radio-SE-HPLC (Superdex 200 Increase 10/300 GL column, 0.75 mL/min flow rate, and PBS pH 7.4 as an eluent).

**Melanoma Cell Lines.** The human melanoma cancer cell line A375-MA1 was purchased from the American Type Culture Collection (ATCC, Manassas, VA) and maintained in Dulbecco's Modified Eagle Medium supplemented with 10% heat-inactivated fetal calf serum, 100 units/mL penicillin, and 100 units/mL streptomycin in an incubator (Heracell 150i, ThermoFisher Scientific) set to 37  $^\circ\text{C}$  and 5%  $\text{CO}_2$ . The cell lines were harvested and passaged upon reaching 80% confluency using 0.25% trypsin/0.53 mM EDTA in Hank's

Buffered Salt Solution without calcium and magnesium. All media was purchased from the Media Preparation Facility at MSKCC.

**Xenograft Models.** Six- to eight-week-old female athymic nude mice were obtained from Charles River Laboratories (Wilmington, MA) and allowed to acclimatize for approximately 1 week prior to inoculation. Animals were housed in ventilated cages and given water and food *ad libitum*. Mice were anaesthetized by inhalation of 2% isoflurane (Baxter Healthcare, Deerfield, IL)/oxygen gas mixture and xenografted subcutaneously on the right flank with  $5 \times 10^6$  A375-MA1 cells in 150  $\mu\text{L}$  of cell suspension of a 1:1 mixture of fresh media/Matrigel (Corning Life Sciences, Corning, NY). The A375-MA1 tumors reached the ideal size for imaging and biodistribution studies ( $\sim 100 \text{ cm}^3$ ) after approximately 2 to 3 weeks. Mice bearing melanoma patient-derived xenograft (PDX)-tumors were received from the MSKCC Anti-Tumor Assessment Core Facility. Three different PDX cell lines were investigated: JW-217a (disease stage: 1Bc T1bN0M0), JW-218a (disease stage: 4), and JW-159a (disease stage: 2c T4bN0M0). The PDXs were inoculated bilaterally, yielding 1–4 tumors of varying sizes per mouse. The PDX tumors reached the ideal size for imaging and biodistribution studies after  $\sim 5$ –6 weeks.

**Immunohistochemistry.** Gal-3BP expression was evaluated by immunohistochemistry (IHC) in harvested tumors from mice. The tumors were snap frozen as optimal cutting temperature (OCT) blocks and cut to 10  $\mu\text{m}$  thick sections. The sections were fixed with acetone (10 min), blocked with 1% bovine serum albumin (BSA) in PBS solution (30 min), and incubated with 1959 (2  $\mu\text{g}/\text{mL}$ , 1 h). Goat anti-human IgG conjugated with AlexaFluor 488 (1:200 dilution, 1 h incubation, A11013, Invitrogen) was used as the secondary antibody.

**PET Imaging.** PET imaging was conducted on a microPET Focus 120 small-animal scanner (Siemens Medical Solutions, Malvern PA). Approximately 5 min prior to PET image acquisition, mice were anaesthetized by inhalation of 2% isoflurane/oxygen gas mixture and kept under anesthesia for the duration of the scan. Static scans were recorded at 24, 48, 72, 96, and 120 h after the intravenous administration of the  $^{89}\text{Zr}$ -labeled immunoconjugates (Table 1). An energy window

**Table 1. Doses of Radioimmunoconjugates Administered to the Mice**

Radioimmunoconjugate	Mass ( $\mu\text{g}$ )	Radioactivity (MBq)	Specific Activity (MBq/mg)
[ $^{89}\text{Zr}$ ]Zr-DFO-1959	6.0–6.7	2.95–3.30	492
[ $^{89}\text{Zr}$ ]Zr-DFO-1959-sss/DM4	6.5–6.7	3.06–3.16	474
[ $^{89}\text{Zr}$ ]Zr-DFO-huIgG	7.2–7.3	2.19–2.20	303

of 350–700 keV and a coincidence timing window of 6 ns were used. Data were sorted into 2-dimensional histograms by Fourier rebinning, and transverse images were reconstructed by filtered back-projection (FBP). The imaging data were then normalized to correct for nonuniformity of response of the detector, physical decay of the radionuclide to the time of injection, dead-time count losses, and positron-branching ratio, but no attenuation, scatter, or partial-volume averaging correction was applied. The counting rates in the reconstructed images were converted to activity concentrations (percentage injected dose per gram of tissue [%ID/g]) using a system

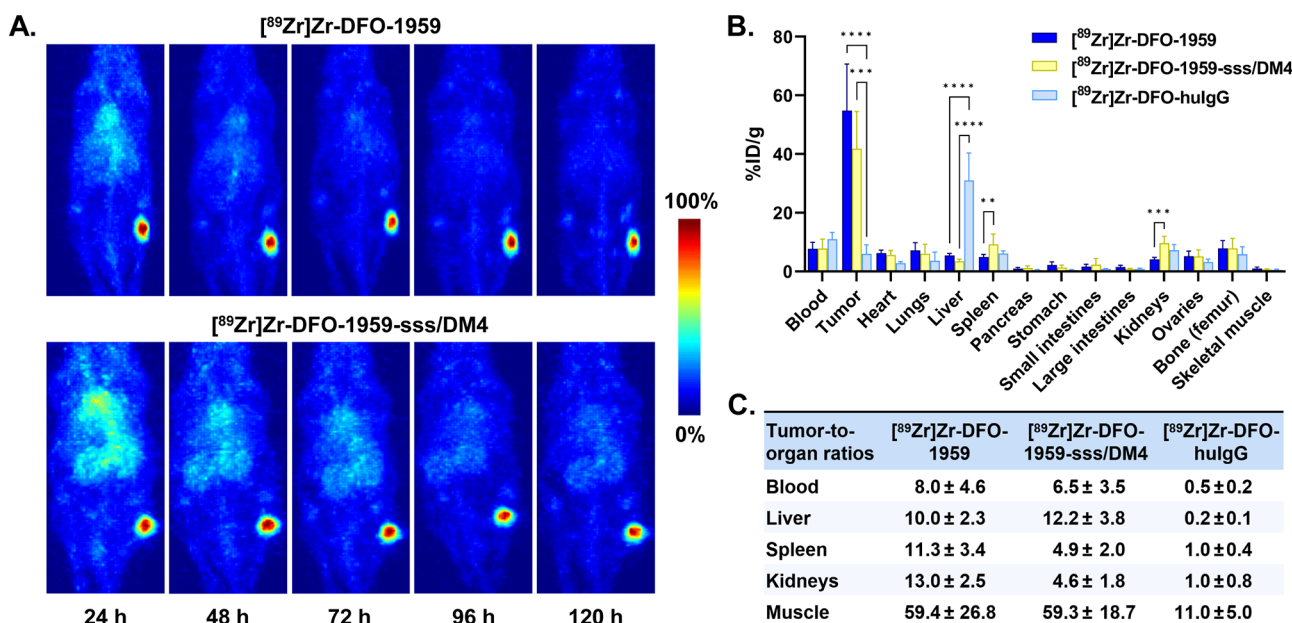


**Figure 1.** Biodistribution of  $[^{89}\text{Zr}]\text{Zr-DFO-1959}$ ,  $[^{89}\text{Zr}]\text{Zr-DFO-1959-sss/DM4}$ , and  $[^{89}\text{Zr}]\text{Zr-DFO-huIgG}$  in mice bearing A375-MA1 tumors. (A) Maximum intensity projection (MIP) PET images of a representative mouse from each cohort acquired at 24, 48, 72, 96, and 120 h after intravenous injection. (B) *Ex vivo* biodistribution of  $[^{89}\text{Zr}]\text{Zr-DFO-1959}$ ,  $[^{89}\text{Zr}]\text{Zr-DFO-1959-sss/DM4}$ , and  $[^{89}\text{Zr}]\text{Zr-DFO-huIgG}$  in selected tissues 120 h post-injection. (C) Selected tumor-to-healthy organ activity concentration ratios at 120 h post-injection.  $P \leq 0.05$  \*,  $P \leq 0.01$  \*\*,  $P \leq 0.001$  \*\*\*, and  $P \leq 0.0001$  \*\*\*\*.

calibration factor derived from the imaging of a mouse-sized water-equivalent phantom containing  $^{89}\text{Zr}$ . Maximum intensity projection (MIP) images were generated from 3-dimensional ordered subset expectation maximization reconstruction (3D-OSEM). The resulting images were analyzed using ASIPro VM software (Concorde Microsystems). Table 1 lists the administered doses to mice.

**Ex Vivo Biodistribution Studies.** Athymic nude mice bearing subcutaneous A375-MA1 (right flank,  $\sim 100 \text{ mm}^3$ ,  $n = 5\text{--}6$  per cohort) were randomized prior to the study and were gently warmed with a heat lamp for 5 min prior to the administration of  $[^{89}\text{Zr}]\text{Zr-DFO-1959}$ ,  $[^{89}\text{Zr}]\text{Zr-DFO-1959-sss/DM4}$ , or  $[^{89}\text{Zr}]\text{Zr-DFO-huIgG}$  via tail vein injection ( $t = 0$ ). Table 1 lists the administered doses.  $[^{89}\text{Zr}]\text{Zr-DFO-1959}$  was also investigated in PDX-bearing mice using the same dose as in the A375-MA1 experiments ( $n = 3\text{--}4$  per cohort). All mice were euthanized via  $\text{CO}_2(\text{g})$  asphyxiation at 120 h post-injection, and selected tissues were collected and placed into preweighed tubes. The mass of each organ was determined, and each sample was then counted using a Wizard<sup>2</sup> automatic gamma counter. Four aliquots (5  $\mu\text{L}$ ) were weighed and counted as internal standards for each radiolabeled construct. The total injected dose was found as the mass injected dose  $\times$  internal standard average counts/g. The percent injected dose (%ID) was determined as the counts for the tissue  $\times 100$ /total injected dose. The %ID/g was calculated as the %ID/tissue mass in g.

**Statistical Analysis.** Statistical differences were analyzed with GraphPad Prism software (9.5 GraphPad Software Inc., San Diego, CA, USA) via one-way analysis of variance (ANOVA) tests.  $P \leq 0.05$  \*,  $P \leq 0.01$  \*\*,  $P \leq 0.001$  \*\*\*, and  $P \leq 0.0001$  \*\*\*\*.

## RESULTS

**Bioconjugation and Radiolabeling.** The bioconjugation of 1959, 1959-sss/DM4, and huIgG produced immunoconjugates with degrees of labeling between 1 and 2 DFO/mAb (Table S1). Subsequent ELISA experiments demonstrated that the ability of 1959 and 1959-sss/DM4 to bind Gal-3BP was not impacted by modification with DFO (Figure S1). The radiolabeling of DFO-1959, DFO-1959-sss/DM4, and huIgG with  $^{89}\text{Zr}$  produced radioimmunoconjugates in high radiochemical yield ( $>80\%$ ) and radiochemical purity ( $>99\%$ ). SE-HPLC before and after modification with DFO revealed little to no aggregation (Figure S2). Finally, radio-iTLC measurements demonstrated that both  $[^{89}\text{Zr}]\text{Zr-DFO-1959}$  and  $[^{89}\text{Zr}]\text{Zr-DFO-1959-sss/DM4}$  remained  $>80\%$  stable to demetalation over 7 days in human serum at 37  $^\circ\text{C}$  (Figure S3).

**Comparing  $[^{89}\text{Zr}]\text{Zr-DFO-1959}$  and  $[^{89}\text{Zr}]\text{Zr-DFO-1959-sss/DM4}$ .** The *in vivo* behavior of  $[^{89}\text{Zr}]\text{Zr-DFO-1959}$  and  $[^{89}\text{Zr}]\text{Zr-DFO-1959-sss/DM4}$  was compared in mice bearing subcutaneous A375-MA1 xenografts to determine if the pharmacokinetic profile of the  $^{89}\text{Zr}$ -labeled mAb accurately reflects that of the  $^{89}\text{Zr}$ -labeled ADC. The data indicate that the radioimmunoconjugates effectively target tumor tissue (Figure 1 and Table S2). At 120 h post-injection, both  $[^{89}\text{Zr}]\text{Zr-DFO-1959}$  and  $[^{89}\text{Zr}]\text{Zr-DFO-1959-sss/DM4}$  produced high tumor uptake ( $54.8 \pm 15.8\% \text{ID/g}$  and  $41.8 \pm 12.7\% \text{ID/g}$ , respectively) compared to only  $6.0 \pm 3.1\% \text{ID/g}$  for  $[^{89}\text{Zr}]\text{Zr-DFO-huIgG}$ , the isotype-specific control. Furthermore, the uptake of both probes in nontarget organs was low at later time points ( $<5\% \text{ID/g}$ ), ultimately yielding promising tumor-to-healthy organ activity concentration ratios. That said, statistically significant differences in uptake were observed in two tissues: the kidneys and the spleen (Figure S4). In the former, the uptake of  $[^{89}\text{Zr}]\text{Zr-DFO-1959-sss/DM4}$  ( $9.7 \pm 2.3\% \text{ID/g}$ ) was double that of  $[^{89}\text{Zr}]\text{Zr-DFO-1959}$  ( $4.9 \pm 2.0\% \text{ID/g}$ ).

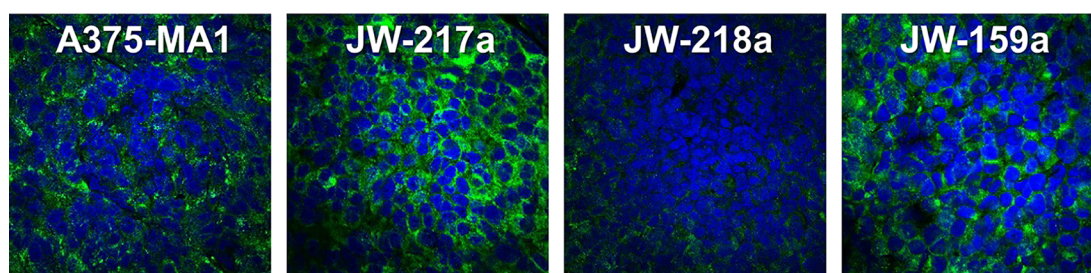


**Figure 2.** Confocal microscopy images of melanoma cell lines stained for Gal-3BP with 1959. Blue: DAPI; Green: Goat antihuman IgG secondary antibody conjugated with AlexaFluor 488.

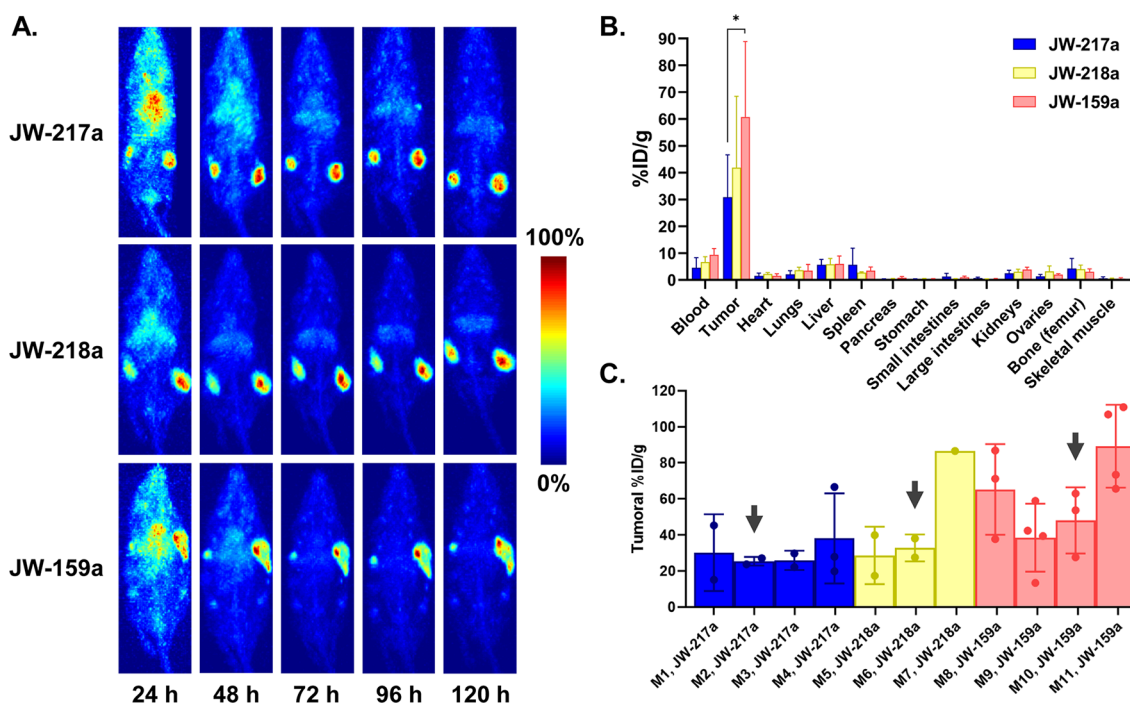


**Figure 3.** Performance of  $[^{89}\text{Zr}]\text{Zr-DFO-1959}$  in PDX models of melanoma. (A) MIP PET images acquired 24, 48, 72, 96, and 120 h after the administration of  $[^{89}\text{Zr}]\text{Zr-DFO-1959}$ . (B) *Ex vivo* biodistribution data collected 120 h after the administration of  $[^{89}\text{Zr}]\text{Zr-DFO-1959}$  (\*  $P = 0.0112$ ). (C) Uptake values for each mouse and tumor. The PDXs were inoculated bilaterally, yielding 1–4 tumors of varying sizes per mouse. Arrows indicate the mice shown in (A).

1959 ( $4.2 \pm 0.6\% \text{ID/g}$ ;  $P$ -value = 0.0002). In the latter, the  $^{89}\text{Zr}$ -labeled ADC likewise produced a higher activity concentration ( $9.3 \pm 3.4\% \text{ID/g}$ ) than the  $^{89}\text{Zr}$ -labeled mAb ( $5.0 \pm 0.9\% \text{ID/g}$ ;  $P$ -value = 0.0096).

**ImmunoPET in Patient-Derived Xenograft Models of Melanoma.** Following the experiments in the mice bearing A375-MA1 xenografts, we next sought to study our radioimmunoconjugates in a more realistic recapitulation human disease: mice bearing patient-derived xenografts (PDXs). To this end, we acquired slides of three melanoma PDXs — JW-217a, JW-218a, and JW-159a — from the Memorial Sloan Kettering Anti-Tumor Assessment Core. All three exhibited Gal-3BP staining on par with the A375-MA1 cells, a finding that aligns with literature reports regarding the expression of Gal-3BP in melanoma (Figures 2 and S5).<sup>25,31</sup>

In light of these *in vitro* data, we moved to interrogate the behavior of  $[^{89}\text{Zr}]\text{Zr-DFO-1959}$  in athymic nude mice bearing subcutaneous PDXs. As shown in Figure 3 and Table S3, the radioimmunoconjugate clearly visualized JW-217a, JW-218a, and JW-159a xenografts with high tumor-to-background contrast. Critically, however, substantial heterogeneity was

observed in the uptake of  $[^{89}\text{Zr}]\text{Zr-DFO-1959}$  in the different PDXs. For example, higher uptake was observed in the JW-159a tumors than the JW-217a xenografts ( $P$ -value: 0.0112). Heterogeneous uptake was also seen between different tumors of a single PDX type in a single mouse (Figure 3C and Table S4). To wit, the four tumors isolated from M11 (JW-159a xenografts) exhibited uptake values ranging from  $\sim 60\% \text{ID/g}$  to  $>100\% \text{ID/g}$ ; M4 (JW-217a xenografts) had tumors with lower but equally heterogeneous uptake values ranging from  $\sim 20\% \text{ID/g}$  to  $\sim 70\% \text{ID/g}$ . Taken together, these data suggest that factors beyond antigen expression levels—perhaps perfusion or stromal density—may also be influencing the accumulation of the radioimmunoconjugate in the tumor tissue.

## DISCUSSION

Two overarching impressions arise from these data: (1)  $[^{89}\text{Zr}]\text{Zr-DFO-1959}$  effectively delineated Gal-3BP-expressing A375-MA1 and patient-derived melanoma xenografts and (2)  $[^{89}\text{Zr}]\text{Zr-DFO-1959}$  and  $[^{89}\text{Zr}]\text{Zr-DFO-1959-sss/DM4}$  displayed similar—but *not* identical—pharmacokinetic profiles in an A375-MA1 xenograft model of melanoma.

The first result clearly suggests that [ $^{89}\text{Zr}$ ]Zr-DFO-1959 could be a useful tool for clinical imaging. Given that Gal-3BP has been linked to poor prognosis, tumor progression, and immune escape in several malignancies, the radioimmunoconjugate could play a role in prognostic imaging. Perhaps even more likely, [ $^{89}\text{Zr}$ ]Zr-DFO-1959 could be used as a companion theranostic agent in support of Gal-3BP-targeted therapies, including ADCs like 1959-sss/DM4. This brings us to the second result. The past two decades have played witness to the advent of ADCs as targeted therapeutics, but the intrinsic heterogeneity of cancer has meant that the prospective identification of patients likely to respond to therapy is of paramount importance. Studies like the ZEPHIR trial underscore the potential of  $^{89}\text{Zr}$ -immunoPET in this regard, but a growing body of evidence suggests that simple radiolabeled antibodies may not be ideal companion imaging agents for ADCs because the latter bear hydrophobic toxins that can alter their pharmacokinetic profiles.<sup>32–35</sup> Indeed, several recent studies have shown that radiolabeled ADCs can have drastically different biodistributions than their parent antibodies, with uptake in both tumor tissue and healthy organs differing substantially.<sup>32–35</sup> This phenomenon has fueled interest in the use of the ADCs themselves as platforms for companion theranostic imaging.<sup>36</sup> In the present study, the biodistributions of [ $^{89}\text{Zr}$ ]Zr-DFO-1959 and [ $^{89}\text{Zr}$ ]Zr-DFO-1959-sss/DM4 were largely similar in athymic nude mice bearing A375-MA1 xenografts, but the latter produced nearly double the uptake in the spleen and kidneys. These data suggest that the pharmacokinetic profile of the  $^{89}\text{Zr}$ -labeled mAb broadly reflects that of 1959-sss/DM4, and thus [ $^{89}\text{Zr}$ ]Zr-DFO-1959 could likely be effectively deployed as a companion theranostic for the ADC. However, further experimentation is needed to determine whether the differences in renal and splenic uptake are substantial enough to affect the ability of the  $^{89}\text{Zr}$ -labeled mAb to predict the clinical efficacy or toxicity of the ADC.

## CONCLUSIONS

Herein, we have described the development of a pair of Gal-3BP-targeting radioimmunoconjugates for  $^{89}\text{Zr}$ -immunoPET: [ $^{89}\text{Zr}$ ]Zr-DFO-1959 and [ $^{89}\text{Zr}$ ]Zr-DFO-1959-sss/DM4. The expression of Gal-3BP by a variety of cancers has made it a particularly enticing target for the development of therapeutics. Our probes demonstrated highly promising *in vivo* behavior in two murine models of melanoma, suggesting that they could ultimately play an important role in the clinic as companion theranostic imaging agents. Moving forward, we aim to explore the utility of [ $^{89}\text{Zr}$ ]Zr-DFO-1959 and [ $^{89}\text{Zr}$ ]Zr-DFO-1959-sss/DM4 for the imaging of cancers other than melanoma, to further interrogate the differences between the *in vivo* behavior of the [ $^{89}\text{Zr}$ ]Zr-mAb and the [ $^{89}\text{Zr}$ ]Zr-ADC, and to investigate the potential of 1959 as a platform for Gal-3BP-targeted radioimmunotherapy with  $\beta$ - and  $\alpha$ -emitting radionuclides.

## ASSOCIATED CONTENT

### Supporting Information

The Supporting Information is available free of charge at <https://pubs.acs.org/doi/10.1021/acs.molpharmaceut.3c00241>.

ELISA results, SE-HPLC chromatograms, *in vitro* stability results, statistical analyses, additional confocal images, and tables of *ex vivo* biodistribution data (PDF)

## AUTHOR INFORMATION

### Corresponding Author

**Brian M. Zeglis** – Department of Chemistry, Hunter College, City University of New York, New York 10021, New York, United States; Department of Radiology, Memorial Sloan Kettering Cancer Center, New York 10065, New York, United States; Ph.D. Program in Biochemistry and Ph.D. Program in Chemistry, Graduate Center of the City University of New York, New York 10016 New York, United States; Department of Radiology, Weill Cornell Medical College, New York 10021, New York, United States; [orcid.org/0000-0002-9091-744X](https://orcid.org/0000-0002-9091-744X); Phone: 212-896-0433; Email: [bz102@hunter.cuny.edu](mailto:bz102@hunter.cuny.edu)

### Authors

**Outi Keinänen** – Department of Chemistry, Hunter College, City University of New York, New York 10021, New York, United States; Department of Chemistry, University of Helsinki, Helsinki 00014, Finland; Department of Radiology, Memorial Sloan Kettering Cancer Center, New York 10065, New York, United States; [orcid.org/0000-0002-3939-6706](https://orcid.org/0000-0002-3939-6706)

**Samantha M. Sarrett** – Department of Chemistry, Hunter College, City University of New York, New York 10021, New York, United States; Department of Radiology, Memorial Sloan Kettering Cancer Center, New York 10065, New York, United States; Ph.D. Program in Biochemistry, Graduate Center of the City University of New York, New York 10016 New York, United States

**Samantha Delaney** – Department of Chemistry, Hunter College, City University of New York, New York 10021, New York, United States; Department of Radiology, Memorial Sloan Kettering Cancer Center, New York 10065, New York, United States; Ph.D. Program in Biochemistry, Graduate Center of the City University of New York, New York 10016 New York, United States

**Cindy Rodriguez** – Department of Chemistry, Hunter College, City University of New York, New York 10021, New York, United States; Department of Radiology, Memorial Sloan Kettering Cancer Center, New York 10065, New York, United States; Ph.D. Program in Chemistry, Graduate Center of the City University of New York, New York 10016 New York, United States

**Eric J. Days** – Department of Chemistry, Hunter College, City University of New York, New York 10021, New York, United States

**Emily Capone** – Department of Innovative Technologies in Medicine & Dentistry, University of Chieti-Pescara, Chieti 66100, Italy; Mediapharma srl, Chieti 66013, Italy; Center for Advanced Studies and Technology, Chieti 66100, Italy

**Frederic Saunier** – Mediapharma srl, Chieti 66013, Italy  
**Rodolfo Ippoliti** – Department of Life, Health and Environmental Sciences, University of L'Aquila, L'Aquila 67100, Italy

**Gianluca Sala** – Department of Innovative Technologies in Medicine & Dentistry, University of Chieti-Pescara, Chieti 66100, Italy; Mediapharma srl, Chieti 66013, Italy; Center for Advanced Studies and Technology, Chieti 66100, Italy

**Stefano Iacobelli** – Mediapharma srl, Chieti 66013, Italy

Complete contact information is available at:

<https://pubs.acs.org/10.1021/acs.molpharmaceut.3c00241>

## Notes

The authors declare the following competing financial interest(s): EC, FS, GS, and SI are employees of Mediapharma srl, which holds intellectual property on the 1959 mAb.

## ACKNOWLEDGMENTS

This work was supported by funding from the Academy of Finland (OMK; Decision No. 331659), the National Institutes of Health (F31CA275334 to SD as well as R01CA240963, U01CA221046, and R01CA244327 to BMZ), Fondazione-AIRC (GS; IG2021 id 25696), and Dept. MeSVA (University of L'Aquila; RI). The authors thank the MSKCC Small Imaging Core Facility and Radiochemistry and Molecular Imaging Probe Core, which are supported by NIH awards P30 CA008748-48, S10 OD016207-01, and S10 RR020892-01. The MSKCC Anti-tumor Assessment Core, Elisa de Stanchina, Omar Hayatt, and Jedd Wolchok are gratefully acknowledged for providing the PDX models.

## ABBREVIATIONS

%ID/g, percent injected dose per gram of tissue; CDX, cell line-derived xenograft; DFO, desferrioxamine; DM4, raptansine (maytansinoid); ELISA, enzyme-linked immunosorbent assay; Gal-3BP, galectin-3 binding protein; HRP, horseradish peroxidase; huIgG, antihuman immunoglobulin G antibody; iTLC, instant thin layer chromatography; mAb, monoclonal antibody; MSKCC, Memorial Sloan Kettering Cancer Center; PDX, patient-derived xenograft; PET, positron emission tomography; PBS, phosphate-buffered saline; RCP, radiochemical purity; SE-HPLC, size exclusion high-performance liquid chromatography; TMB, 3,3',5,5'-tetramethylbenzidine

## REFERENCES

- (1) Iacobelli, S.; Arnò, E.; D'Orazio, A.; Coletti, G. Detection of antigens recognized by a novel monoclonal antibody in tissue and serum from patients with breast cancer. *Cancer Res.* **1986**, *46* (6), 3005–10.
- (2) Ullrich, A.; Sures, I.; D'Egidio, M.; Jallal, B.; Powell, T. J.; Herbst, R.; Dreps, A.; Azam, M.; Rubinstein, M.; Natoli, C.; et al. The secreted tumor-associated antigen 90K is a potent immune stimulator. *J. Biol. Chem.* **1994**, *269* (28), 18401–7.
- (3) Marchetti, A.; Tinari, N.; Buttitta, F.; Chella, A.; Angeletti, C. A.; Sacco, R.; Mucilli, F.; Ullrich, A.; Iacobelli, S. Expression of 90K (Mac-2 BP) correlates with distant metastasis and predicts survival in stage I non-small cell lung cancer patients. *Cancer Res.* **2002**, *62* (9), 2535–9.
- (4) Tinari, N.; Lattanzio, R.; Querzoli, P.; Natoli, C.; Grassadonia, A.; Alberti, S.; Hubalek, M.; Reimer, D.; Nenci, I.; Bruzzi, P.; Piantelli, M.; Iacobelli, S. High expression of 90K (Mac-2 BP) is associated with poor survival in node-negative breast cancer patients not receiving adjuvant systemic therapies. *Int. J. Cancer* **2009**, *124* (2), 333–8.
- (5) Läubli, H.; Alisson-Silva, F.; Stanczak, M. A.; Siddiqui, S. S.; Deng, L.; Verhagen, A.; Varki, N.; Varki, A. Lectin galactoside-binding soluble 3 binding protein (LGALS3BP) is a tumor-associated immunomodulatory ligand for CD33-related Siglecs. *J. Biol. Chem.* **2014**, *289* (48), 33481–91.
- (6) Capone, E.; Iacobelli, S.; Sala, G. Role of galectin 3 binding protein in cancer progression: a potential novel therapeutic target. *J. Transl. Med.* **2021**, *19* (1), 405.
- (7) Iacobelli, S.; Sismondi, P.; Gai, M.; D'Egidio, M.; Tinari, N.; Amatetti, C.; Di Stefano, P.; Natoli, C. Prognostic value of a novel circulating serum 90K antigen in breast cancer. *Br. J. Cancer* **1994**, *69* (1), 172–6.

- (8) Piccolo, E.; Tinari, N.; Semeraro, D.; Traini, S.; Fichera, I.; Cumashi, A.; La Sorda, R.; Spinella, F.; Bagnato, A.; Lattanzio, R.; D'Egidio, M.; Di Risio, A.; Stampolidis, P.; Piantelli, M.; Natoli, C.; Ullrich, A.; Iacobelli, S. LGALS3BP, lectin galactoside-binding soluble 3 binding protein, induces vascular endothelial growth factor in human breast cancer cells and promotes angiogenesis. *J. Mol. Med. (Berl)* **2013**, *91* (1), 83–94.

- (9) Stampolidis, P.; Ullrich, A.; Iacobelli, S. LGALS3BP, lectin galactoside-binding soluble 3 binding protein, promotes oncogenic cellular events impeded by antibody intervention. *Oncogene* **2015**, *34* (1), 39–52.

- (10) Zhang, X.; Ding, H.; Lu, Z.; Ding, L.; Song, Y.; Jing, Y.; Hu, Q.; Dong, Y.; Ni, Y. Increased LGALS3BP promotes proliferation and migration of oral squamous cell carcinoma via PI3K/AKT pathway. *Cell Signal* **2019**, *63*, 109359.

- (11) Inohara, H.; Raz, A. Identification of human melanoma cellular and secreted ligands for galectin-3. *Biochem. Biophys. Res. Commun.* **1994**, *201* (3), 1366–75.

- (12) Sasaki, T.; Brakebusch, C.; Engel, J.; Timpl, R. Mac-2 binding protein is a cell-adhesive protein of the extracellular matrix which self-assembles into ring-like structures and binds beta1 integrins, collagens and fibronectin. *Embo j* **1998**, *17* (6), 1606–13.

- (13) Mariscal, J.; Fernandez-Puente, P.; Calamia, V.; Abalo, A.; Santacana, M.; Matias-Guiu, X.; Lopez-Lopez, R.; Gil-Moreno, A.; Alonso-Alconada, L.; Abal, M. Proteomic Characterization of Epithelial-Like Extracellular Vesicles in Advanced Endometrial Cancer. *J. Proteome Res.* **2019**, *18* (3), 1043–1053.

- (14) Xu, R.; Greening, D. W.; Chen, M.; Rai, A.; Ji, H.; Takahashi, N.; Simpson, R. J. Surfaceome of Exosomes Secreted from the Colorectal Cancer Cell Line SW480: Peripheral and Integral Membrane Proteins Analyzed by Proteolysis and TX114. *Proteomics* **2019**, *19* (8), 1700453.

- (15) Bandu, R.; Oh, J. W.; Kim, K. P. Mass spectrometry-based proteome profiling of extracellular vesicles and their roles in cancer biology. *Exp. Mol. Med.* **2019**, *51* (3), 1–10.

- (16) Han, L.; Lam, E. W.; Sun, Y. Extracellular vesicles in the tumor microenvironment: old stories, but new tales. *Mol. Cancer* **2019**, *18* (1), 59.

- (17) Capone, E.; Lamolinara, A.; Pastorino, F.; Gentile, R.; Ponziani, S.; Di Vittorio, G.; D'Agostino, D.; Bibbò, S.; Rossi, C.; Piccolo, E.; Iacobelli, V.; Lattanzio, R.; Panella, V.; Sallèse, M.; De Laurenzi, V.; Giansanti, F.; Sala, A.; Iezzi, M.; Ponzoni, M.; Ippoliti, R.; Iacobelli, S.; Sala, G. Targeting Vesicular LGALS3BP by an Antibody-Drug Conjugate as Novel Therapeutic Strategy for Neuroblastoma. *Cancers (Basel)* **2020**, *12* (10), 2989.

- (18) Giansanti, F.; Capone, E.; Ponziani, S.; Piccolo, E.; Gentile, R.; Lamolinara, A.; Di Campli, A.; Sallèse, M.; Iacobelli, V.; Cimini, A.; De Laurenzi, V.; Lattanzio, R.; Piantelli, M.; Ippoliti, R.; Sala, G.; Iacobelli, S. Secreted Gal-3BP is a novel promising target for non-internalizing Antibody-Drug Conjugates. *J. Controlled Release* **2019**, *294*, 176–184.

- (19) Gébleux, R.; Stringhini, M.; Casanova, R.; Soltermann, A.; Neri, D. Non-internalizing antibody-drug conjugates display potent anti-cancer activity upon proteolytic release of monomethyl auristatin E in the subendothelial extracellular matrix. *Int. J. Cancer* **2017**, *140* (7), 1670–1679.

- (20) Dal Corso, A.; Gébleux, R.; Murer, P.; Soltermann, A.; Neri, D. A non-internalizing antibody-drug conjugate based on an anthracycline payload displays potent therapeutic activity in vivo. *J. Controlled Release* **2017**, *264*, 211–218.

- (21) Szot, C.; Saha, S.; Zhang, X. M.; Zhu, Z.; Hilton, M. B.; Morris, K.; Seaman, S.; Dunleavy, J. M.; Hsu, K. S.; Yu, G. J.; Morris, H.; Swing, D. A.; Haines, D. C.; Wang, Y.; Hwang, J.; Feng, Y.; Welsch, D.; DeCrescenzo, G.; Chaudhary, A.; Zudaire, E.; Dimitrov, D. S.; St Croix, B. Tumor stroma-targeted antibody-drug conjugate triggers localized anticancer drug release. *J. Clin. Invest.* **2018**, *128* (7), 2927–2943.

(22) Khongorzul, P.; Ling, C. J.; Khan, F. U.; Ihsan, A. U.; Zhang, J. Antibody-Drug Conjugates: A Comprehensive Review. *Mol. Cancer Res.* **2020**, *18* (1), 3–19.

(23) Tong, J. T. W.; Harris, P. W. R.; Brimble, M. A.; Kavianinia, I. An Insight into FDA Approved Antibody-Drug Conjugates for Cancer Therapy. *Molecules* **2021**, *26* (19), 5847.

(24) van Dongen, G.; Beaino, W.; Windhorst, A. D.; Zwezerijnen, G. J. C.; Oprea-Lager, D. E.; Hendrikse, N. H.; van Kuijk, C.; Boellaard, R.; Huisman, M. C.; Vugts, D. J. The Role of  $^{89}\text{Zr}$ -Immuno-PET in Navigating and Derisking the Development of Biopharmaceuticals. *J. Nucl. Med.* **2021**, *62* (4), 438–445.

(25) Ferrucci, P. F.; Cocorocchio, E. Novel Biomarkers and Druggable Targets in Advanced Melanoma. *Cancers (Basel)* **2022**, *14* (1), 81.

(26) Gebhart, G.; Lamberts, L. E.; Wimana, Z.; Garcia, C.; Emonts, P.; Ameye, L.; Stroobants, S.; Huizing, M.; Aftimos, P.; Tol, J.; Oyen, W. J.; Vugts, D. J.; Hoekstra, O. S.; Schröder, C. P.; Menke-van der Houven van Oordt, C. W.; Guiot, T.; Brouwers, A. H.; Awada, A.; de Vries, E. G.; Flamen, P. Molecular imaging as a tool to investigate heterogeneity of advanced HER2-positive breast cancer and to predict patient outcome under trastuzumab emtansine (T-DM1): the ZEPHIR trial. *Ann. Oncol.* **2016**, *27* (4), 619–24.

(27) Sharma, S. K.; Sevak, K. K.; Monette, S.; Carlin, S. D.; Knight, J. C.; Wuest, F. R.; Sala, E.; Zeglis, B. M.; Lewis, J. S. Preclinical  $^{89}\text{Zr}$  Immuno-PET of High-Grade Serous Ovarian Cancer and Lymph Node Metastasis. *J. Nucl. Med.* **2016**, *57* (5), 771–6.

(28) Jansen, M. H.; Lagerweij, T.; Sewing, A. C.; Vugts, D. J.; van Vuurden, D. G.; Molthoff, C. F.; Caretti, V.; Veringa, S. J.; Petersen, N.; Carcaboso, A. M.; Noske, D. P.; Vandertop, W. P.; Wesseling, P.; van Dongen, G. A.; Kaspers, G. J.; Hulleman, E. Bevacizumab Targeting Diffuse Intrinsic Pontine Glioma: Results of  $^{89}\text{Zr}$ -Bevacizumab PET Imaging in Brain Tumor Models. *Mol. Cancer Ther.* **2016**, *15* (9), 2166–74.

(29) Lohrmann, C.; O'Reilly, E. M.; O'Donoghue, J. A.; Pandit-Taskar, N.; Carrasquillo, J. A.; Lyashchenko, S. K.; Ruan, S.; Teng, R.; Scholz, W.; Maffiuid, P. W.; Lewis, J. S.; Weber, W. A. Retooling a Blood-Based Biomarker: Phase I Assessment of the High-Affinity CA19–9 Antibody HuMab-SB1 for Immuno-PET Imaging of Pancreatic Cancer. *Clin. Cancer Res.* **2019**, *25* (23), 7014–7023.

(30) McDonagh, C. F.; Turcott, E.; Westendorf, L.; Webster, J. B.; Alley, S. C.; Kim, K.; Andreyka, J.; Stone, I.; Hamblett, K. J.; Francisco, J. A.; Carter, P. Engineered antibody–drug conjugates with defined sites and stoichiometries of drug attachment. *Protein Engineering, Design and Selection* **2006**, *19* (7), 299–307.

(31) Inohara, H.; Raz, A. Identification of Human Melanoma Cellular and Secreted Ligands for Galectin-3. *Biochem. Biophys. Res. Commun.* **1994**, *201* (3), 1366–1375.

(32) Al-Saden, N.; Lam, K.; Chan, C.; Reilly, R. M. Positron-Emission Tomography of HER2-Positive Breast Cancer Xenografts in Mice with ( $^{89}\text{Zr}$ -Labeled Trastuzumab-DM1): A Comparison with ( $^{89}\text{Zr}$ -Labeled Trastuzumab. *Mol. Pharmaceutics* **2018**, *15* (8), 3383–3393.

(33) Chomet, M.; Schreurs, M.; Nguyen, M.; Howng, B.; Villanueva, R.; Krimm, M.; Vasiljeva, O.; van Dongen, G.; Vugts, D. J. The tumor targeting performance of anti-CD166 Probody drug conjugate CX-2009 and its parental derivatives as monitored by  $^{89}\text{Zr}$ -immuno-PET in xenograft bearing mice. *Theranostics* **2020**, *10* (13), 5815–5828.

(34) Jacobson, O.; Li, Q.; Chen, H.; Niu, G.; Kiesewetter, D. O.; Xu, L.; Cook, K.; Yang, G.; Dall'Acqua, W.; Tsui, P.; Peng, L.; Chen, X. PET-Guided Evaluation and Optimization of Internalized Antibody-Drug Conjugates Targeting Erythropoietin-Producing Hepatoma A2 Receptor. *J. Nucl. Med.* **2017**, *58* (11), 1838–1844.

(35) Kang, L.; Jiang, D.; Ehlerding, E. B.; Barnhart, T. E.; Ni, D.; Engle, J. W.; Wang, R.; Huang, P.; Xu, X.; Cai, W. Noninvasive Trafficking of Brentuximab Vedotin and PET Imaging of CD30 in Lung Cancer Murine Models. *Mol. Pharmaceutics* **2018**, *15* (4), 1627–1634.

(36) Adumeau, P.; Vivier, D.; Sharma, S. K.; Wang, J.; Zhang, T.; Chen, A.; Agnew, B. J.; Zeglis, B. M. Site-Specifically Labeled

Antibody-Drug Conjugate for Simultaneous Therapy and Immuno-PET. *Mol. Pharmaceutics* **2018**, *15* (3), 892–898.

## Recommended by ACS

### Novel [ $^{111}\text{In}$ ]In-BnDTPA-EphA2-230-1 Antibody for Single-Photon Emission Computed Tomography Imaging Tracer Targeting of EphA2

Takenori Furukawa, Hiroyuki Yasui, *et al.*

FEBRUARY 09, 2023  
ACS OMEGA

READ 

### Evaluation of a CD206-Targeted Peptide for PET Imaging of Macrophages in Syngeneic Mouse Models of Cancer

Candace C. Parker, Suzanne E. Lapi, *et al.*

APRIL 04, 2023  
MOLECULAR PHARMACEUTICS

READ 

### Gallium-68-Labeled $Z_{\text{PDGFR}\beta}$ Affibody: A Potential PET Probe for Platelet-Derived Growth Factor Receptor $\beta$ -Expressing Carcinomas

Xin Li, Rong Tian, *et al.*

JANUARY 24, 2023  
MOLECULAR PHARMACEUTICS

READ 

### Clickable Shiga Toxin B Subunit for Drug Delivery in Cancer Therapy

Natalia Danielewicz, Juergen Mairhofer, *et al.*

APRIL 18, 2023  
ACS OMEGA

READ 

Get More Suggestions >